SMAR 2017 – Fourth Conference on Smart Monitoring,
Assessment and Rehabilitation of Civil Structures

Optical and Acoustic Techniques for Crack Monitoring in RC Building Structures

WATANABE Toru [1], YANASE Takahito [2], TAKAHASHI Noriyuki [3], OGATA Yoshihiro [4], SAKURAI Masato [5], and KOBAYASHI Jun [5]

[1] Obayashi Corporation, Tokyo, Japan
[2] Just Co.,Ltd., Yokohama, Japan
[3] Tohoku University, Sendai, Japan
[4] Tohoku Electric Power Co.,Inc., Sendai, Japan
[5] Akita Prefectural University, Yurihonjo, Japan

ABSTRACT: Two methods utilizing Optical Image Digitization and Acoustic Emission (AE) Technique are examined as tools for the Structural Health Monitoring (SHM) of reinforced concrete (RC) walls. Wall surfaces are captured as 240 mega-pixel digital images from moment to moment. Cracks in each image are recognized as pixels in lower luminance value compared to un-cracked surfaces. Analyzing the shapes of the masses of lower luminance pixels, cracks and pores are discriminated from each other. The AE system consists of acoustic sensors, analyzing computer and communication devices connecting these to each other. In this method, 4 thresholds are preset to the levels of signals in every 0.0001sec, and the counted number of signals within each threshold in the interval of 1.0sec is used for judging the signals caused by cracking or other noise. Both are examined and verified through the actual loading tests of RC wall specimens with highly accurate loading control and measuring systems.

1 INTRODUCTION

Recently, huge earthquakes have frequently occurred in Japan. A SHM for buildings and structures is considered to be helpful to achieve Business Continuity Plan (BCP) before and/or after those quakes. The earthquakes may cause a damage (or damages) to the buildings and structures and affect its safety by changing the dynamic properties of RC structures which are designed considering their nonlinear behaviors. The influence of minor cracks including hair cracks due to drying or aging on mechanical properties of RC walls has not been investigated sufficiently so far. The relation between the nonlinearity and the occurrence of cracks is not clear in the very small deformation range in particular.

In this paper, two methods utilizing Optical Image Digitization and AE Technique are examined as tools for the Structural Health Monitoring of RC walls. Both methods are verified through the actual static loading tests of RC wall specimens using highly accurate loading control and measuring systems.

2 STRUCTURAL HEALTH MONITORING

2.1 Optical Image Digitization

In measurement of crack widths using Optical Image Digitization methods, the optical image of wall surfaces captured by cameras are obtained as 240 mega-pixel digital images at positive/negative peaks and unloaded stages in each loading cycle. In total of 12 cameras are placed on a frame at an interval in order to cover the whole area of specimen, and the resolution of the digital image corresponds to 0.08mm per pixel, therefore the minimum detectable width of crack is 0.5pixel = 0.04mm in principle. Cracks in each image are recognized as pixels in lower luminance value compared to un-cracked surfaces. By analyzing the shapes of such pixels, cracks are discriminated from pores, which also show lower luminance value, so that the growth of cracks on the surface of RC walls can be monitored.

Crack locations are identified by processing digital images. Trimming of unnecessary pixels from an image, reduction of noise, extraction of pixels which are assumed to be a crack and measurement of the crack width are performed in a series of process. For example, a result of the treatment process to identify cracks is shown in Figure 1.

2.2 Acoustic Emission Technique

AE Technique system is adopted to detect occurrence of cracks. The system consists of "Smart" AE sensors (SAE) and analyzing computer. The system is shown in Figure 2. It is a well-known fact that cracking in brittle materials causes emission of high frequency elastic waves (AE signal), which should be detected separately from other noises. In this method, 4 thresholds are preset to 4 different levels of amplitude (TH1 through TH4 from low to high), and AE signals received in every 0.0001sec are classified into 4 levels. The accumulated and recorded number of AE signal (AE counts) within each threshold in the interval of 1.0sec is used to decide if the waves are caused by cracking.

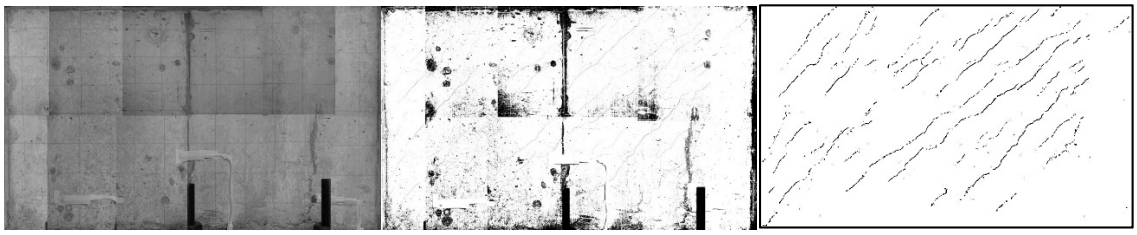

(Left: Original optical image, Center: Two-valued optical image, Right: Noise-eliminated optical image)

Figure 1. A Result of Treatment Process of Optical Image

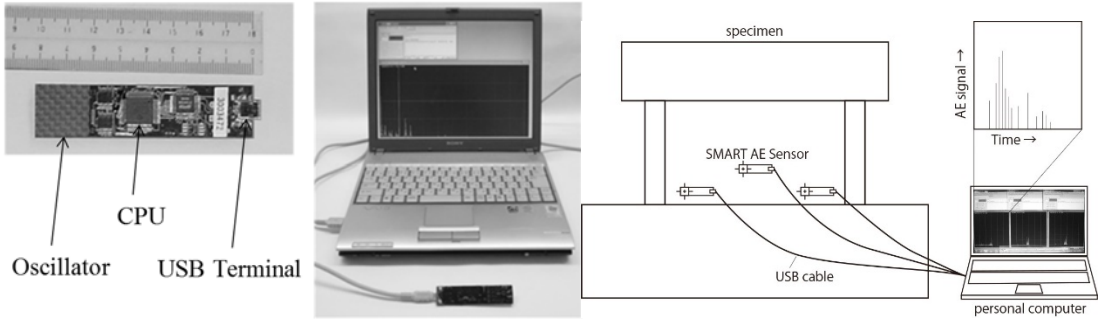

Figure 2. AE Technique system by "Smart" AE sensors (SAE) and Analyzing Computer

3 LOADING TESTS OF RC WALL SPECIMENS

3.1 Outline of Static Loading Tests

SHM is tried for the cyclic loading tests focusing on nonlinearity of RC shear walls which have different initial conditions with and without preset cracks. The amplitude of the loading is ranged from the very small shearing deformation to the failure of the specimen. In each case and step, the relation between the load and the deformation is obtained as the restoring force characteristics to estimate the stiffness degradation. The corresponding data by the image digitization and SAE sensors are examined with those characteristics. Section and material properties of 4 specimens are shown in Tables 1 and 2 while configuration of the specimen in Figure 3. The section properties for all the 4 specimens are the same. Loading is controlled by displacement for specimens WCD, WCO1 and WCO2 and by stress for WCS. WCO1 has cross shaped preset cracks and WCO2 has diagonal preset cracks. AE sensors (No.1, No.2 and No.3) are attached to the specimens as shown in Figure 3.

The Loading system is shown in Figure 4. The tests were conducted at Structural Experiment Lab in special experiment building in Akita Prefectural University, Akita, Japan. The specimens are fixed on to the reaction floor with PC steel bars, and horizontal cyclic loading in both positive and negative directions are performed using two respective oil jacks (push by 1,000kN, pull by 500kN) fixed on the reaction frames. Loading menu is shown in Table 3. In this test, loading was performed repeatedly for 5 cycles after 2 cycles of loading with the initial deformation of R=1/10,000rad and 1/5,000rad until the deformation of R=1/1,000rad was achieved. In addition, for the purpose of examining the stiffness reduction behavior at small to medium amplitude, 4 cycles of loading in total were performed in the course of tests as inner loops at the loading steps 4 and 5.

3.2 Results of loading tests

Shear force and displacement (Q-δ) relationship for WCS is shown in Figure 5 representatively. Based on the result that the shear deformation is more predominant to the bending in every specimen, the shearing behaviors are examined further in detail. Hysteresis loops of shear stress and strain (τ-γ) relationships for specimen WCO1 are illustrated in Figure 6, divided in three steps (3-9, 10-11 and 12-14 cycles). In this range it can be seen that the shape of cyclic curve depends on the maximum deformation ever reached. In the case of cyclic loading without occurrence of new cracks in the process, the curve shows upward gradient almost along preceding loading loops with slightly reduced stresses. The tendency can be seen clearly by comparing the shape of inner loop for 10-11 cycles with that for 3-9 cycles.

The stiffness reduction with increasing deformation amplitude is shown in Figure 7. The plots show a shift of secant stiffness calculated from the positive and the negative peak load and the corresponding deformation of each cycle based on the initial stiffness at the first cycle. The label “loading steps” on the horizontal axis expresses a whole sequent of loading cycles having uniform amplitude, corresponding to the deformation amplitude (target load value) shown in the figure. The change of stiffness reduction rate from 9th to 10th step is relatively high in the process after 7th step for all specimens. The difference of the reduction rate change between WCD, WCS and other specimens is significantly small through all the steps. This means the impact on structural basic property derived from the difference of the specimens and the loading control method is quite small.

Development of concrete cracks by visual observation is shown in Figure 8, after the completion of loading for the deformation angles of R=1/3,333rad. and 1/2,500rad. in

specimens WCS and WCO2. Cracking occurred due to loading in positive direction is shown in thick line and in negative in thin line. Cracks developed in tensile against loading at steps with small deformation angles and cracks developed on compression side at steps with larger deformation angles are observed in every specimen. The cracks on compression side for WCS occurred at the deformation angle of R=1/2,500rad. and those for WCO2 occurred at R=1/3,333rad.

Table 1. Section Properties of Specimen

		WCD	WCS	WCO1	WCO2
Loading Control Method		Displacement	Stress	Displacement	Displacement
Preset Crack		None	None	Cross Shape	Diagonal
Flange Wall	BxD	700x150			
	Main Rebar	16-D16	(pg=2.8%)		
	Hoop	2-D10@100	(ps=0.95%)		
Web Wall	Wall Thickness	100			
	Vert. and Hori. Rebar	D10@100	each face (ps=1.4% in both Vert. and Hori.)		

Table 2a. Material Properties of Specimen (Rebar)

Size (property)	Location	Yield Point (N/mm^2)	Young's Modulus (kN/mm^2)	Tensile Strength (N/mm^2)
D10 (SD295A)	Wall Rebar	377	183	504
D16 (SD295A)	Column Main Rebar	371	191	532

Table 2b. Material Properties of Specimen (Concrete)

		WCD	WCS	WCO1	WCO2	Young's Modulus Counts
σ_B	N/mm^2	27.6	28.3	31.2	31.3	31.7
age	Day	28	39	46	52	62
Young's Modulus	kN/mm^2	31.1	31.1	31.1	31.1	
Poisson's Ratio		0.203	0.203	0.203	0.203	

Table 3a. Loading Menu (Step 1-7)

Deformation Angle (rad.)	Displacement δ (mm)	Loading Step
1/10,000	0.100	1
1/5,000	0.200	2
1/3,333	0.300	3
1/5,000'	0.200	4
1/3,333'	0.300	5
1/2,500	0.400	6
1/1,667	0.600	7

Table 3b. Loading Menu (Step 8-)

Deformation Angle (rad.)	Displacement δ (mm)	Loading Step
1/1,250	0.800	8
1/1,000	1.000	9
1/500	2.000	10
1/333	3.000	11
1/250	4.000	12 (or Push-Over)
1/200	5.000	Push-Over
1/133	7.500	Push-Over

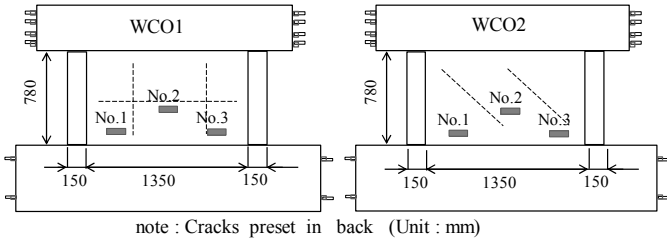

Figure 3. Configuration of Specimen

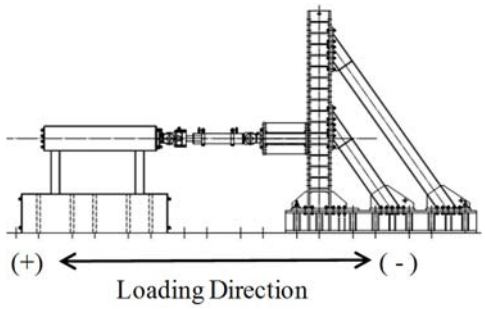

Figure 4. Loading System

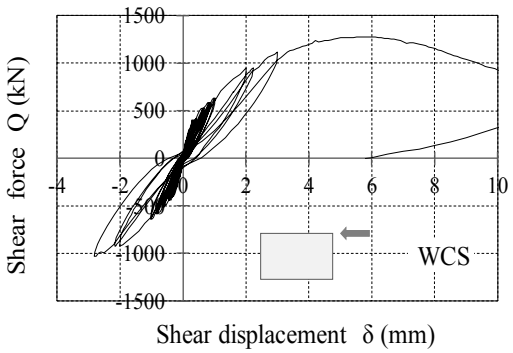

Figure 5. Q-δ relationship for Specimen WCS

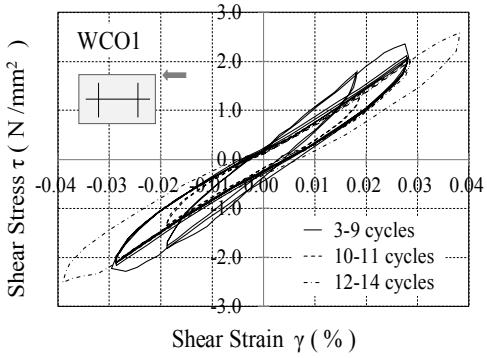

Figure 6. τ-γ relationships for Specimen WCO1

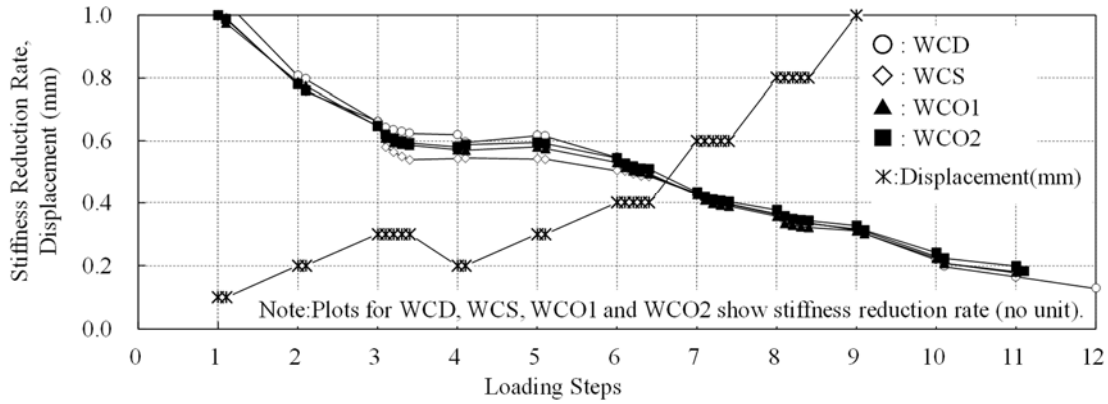

Figure 7. Stiffness Reduction Rate with Increasing Deformation Amplitude

Deformation Angle (rad.)	WCS (Preset Crack: None)	WCO2 (Preset Crack: Diagonal [dashed line])
1/3,333 (δ=0.3mm)	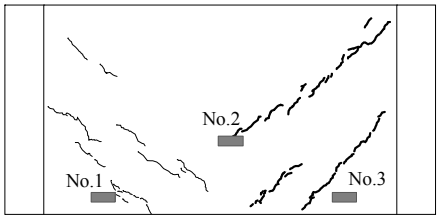	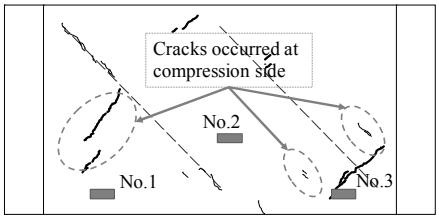
1/2,500 (δ=0.4mm)	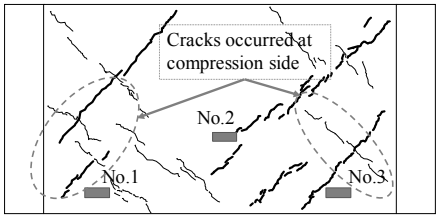	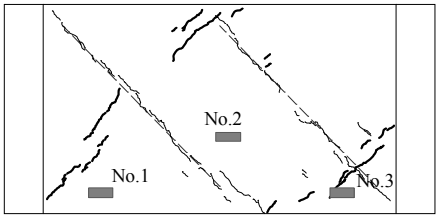

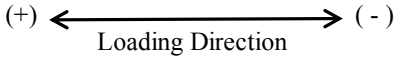

Thick line: Cracks due to positive loading(+) Thin line: Cracks due to negative loading(-)

Figure 8. Development of Concrete Cracks (Upper: R=1/3,333rad. Lower: R=1/2,500rad.)

4 RESULTS OF OPTICAL DIGITAL MONITORING

4.1 Maximum crack widths in very small deformation range

Maximum crack widths due to initial cyclic loadings in very small deformation range are shown in Figure 9. The maximum crack widths of the specimens with preset cracks (WCO1 and WCO2) are apt to be smaller than those of specimens without preset cracks (WCD and WCS) because cracks in WCO1 or WCO2 were induced to develop intensively on preset cracks.

4.2 Residual maximum crack widths at unloaded condition

Residual maximum crack widths at unloaded condition are shown in Figure 10. Residual crack occurs at a deformation angle of R=1/500rad in each specimen.

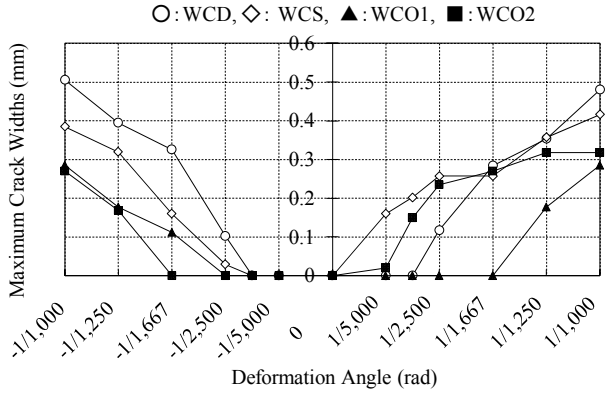

Figure 9. Maximum Crack Widths due to Initial Cyclic Loadings

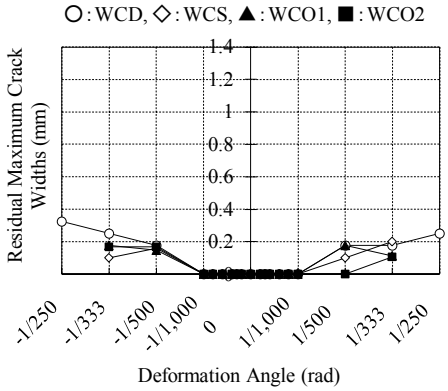

Figure 10. Residual Maximum Crack Widths at Unloaded Condition

5 RESULTS OF ACOUSTIC EMISSION MONITORING

5.1 AE counts time history

Shift of AE counts obtained from sensor No.1 on WCS is shown in Figure 11. This figure shows the relationship between the horizontal deformation and the measuring steps overlaid with AE counts (for threshold value TH2) in bar graph. AE is detected at the negative loading of R=1/5,000rad. (δ=0.2mm) which is before visual observation of cracking, and AE due to shear cracking is much more detected in the vicinity of the AE sensors at negative loading of R=1/3,333rad. eliminating the influence of the noise. Detection number of AE shows rapid increase at R=1/500rad. (Loading Step 10) when the cracks are developed all over the wall.

5.2 Effects of cyclic loading

The relationship between loading cycles and AE counts obtained from sensor No.2 on WCO2 is shown in Figure 12. AE counts observed in the first step of cyclic loading tend to be high. This means that a large number of cracks have occurred at the beginning of new deformation.

5.3 Effects of preset cracks

The points where AE was observed are plotted using circle marks on the P-δ relationship for each specimen in Figure 13. The plotted circle marks correspond to the threshold showing the

largest amplitude observed at the measuring point (TH2: white, TH3: gray and TH4: black). The results for TH2 are especially focused to compare the difference.

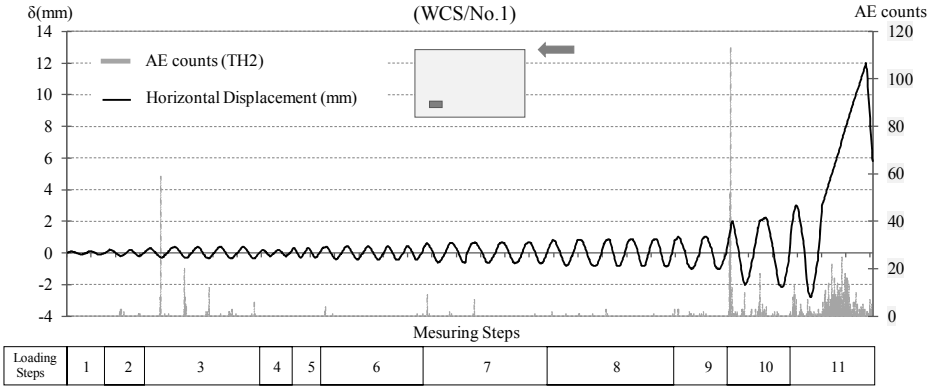

Figure 11. Relationship between Horizontal Deformation and AE counts (TH2)

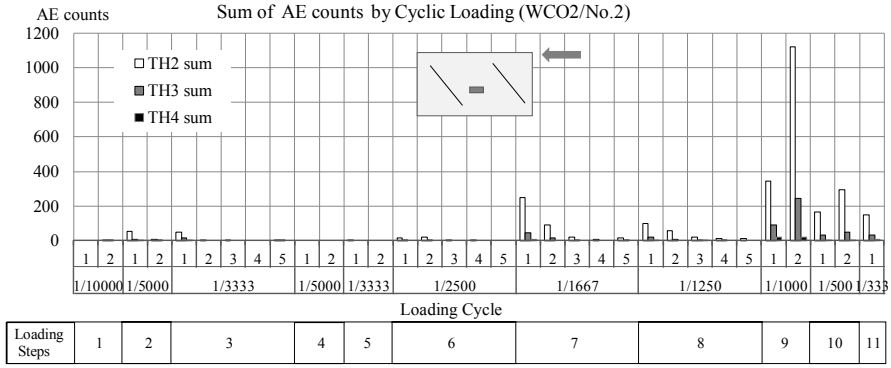

Figure 12. Relationship between Loading Cycles and AE counts

AE sensors	WCS (Preset Crack: None)	WCO2 (Preset Crack: Diagonal)
No.1	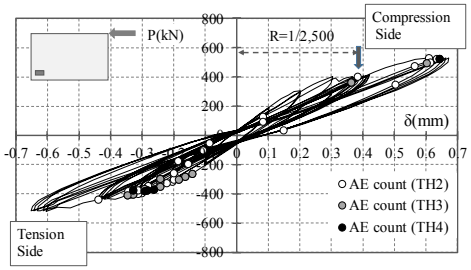	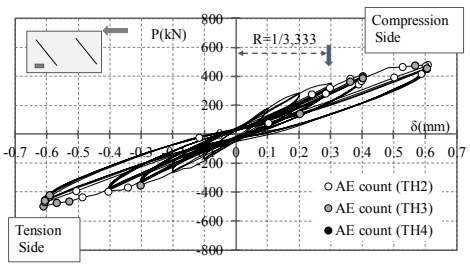
No.3	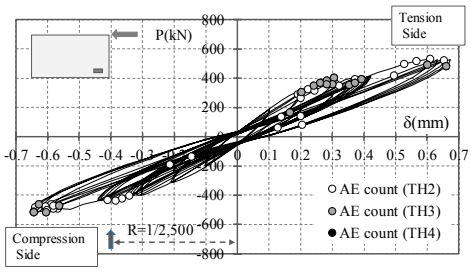	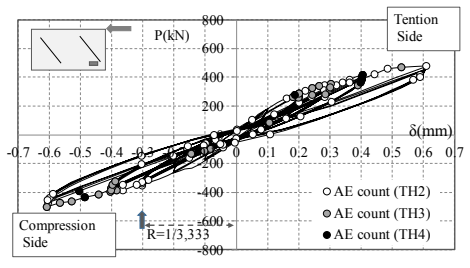

Figure 13. AE Counts on P-δ relationships

Cracking on compression side of WCS occurred at positive and negative loading of deformation angle of R=1/2,500rad. (refer to Figure 8). The sensor No.1 located on compression side at positive loading observed AE of TH2 at positive loading of R=1/2,500rad. while No.3 located on compression side at negative loading observed AE of TH2 at negative loading of R=1/2,500rad. Cracking on compression side of WCO2 occurred at positive and negative loading of R=1/3,333rad. (refer to Figure 8). The sensor No.1 located on compression side at positive loading observed AE of TH2 at positive loading of R=1/3,333rad. while No.3 located on compression side at negative loading observed AE of TH2 at negative loading of R=1/3,333rad.

The AE results corresponds well to the occurrence of cracking for both specimens and show the difference in the initial conditions of the specimen reasonably.

6 DISCUSSIONS

In the cyclic loading tests, by processing the optical images of wall surface, cracks are clearly detected with its width amplified corresponding to increase of deformation. Such relation depends on the existence of the preset cracks; however, improvement of the analytical method may be necessary to extract real cracks through developing better noise reduction technique. As shown in Figure 10, residual cracks occur at R=1/500rad. in every specimen, which is consistent with the result that the change of stiffness reduction rate after 7th step (R=1/1,667rad.) becomes maximum at 10th step (R=1/500rad.) shown in Figure 7.

The AE system is capable to detect occurrence of invisible cracks in very small deformation range. AE sensors count the number of AE wave exceeding thresholds which are assumed to be sufficient to eliminate the influence of the noise. AE counts show good agreement with the occurrence and the extension of the cracks during the cyclic loading. The AE results reflect the difference in the initial conditions of the shear wall specimens. As shown in Figure 12, AE counts at the steps before 9th (R=1/1,000rad) show high value for the first cycle of loading and much lower value for the second cycle or latter. The tendency is consistent with the results shown in Figure 7 that the stiffness is reduced significantly in the first cycle of loading step and slowly in the second cycle or latter.

7 SUMMARY

Two methods utilizing Optical Image Digitization and AE Technique are examined and verified as tools for SHM of reinforced concrete walls. SHM system is expected to judge and detect the damage quickly and securely during/after an earthquake. More practical system is required to be developed in order to apply to actual buildings. We believe the system utilizing Optical Image Digitization and AE Technique could have good prospects in the near future.

References

K.En, M.Nakamura, T.Yanase, S.Ikegaya, and K.Yoneyama, 2010, “Structural Health Monitoring System Applied to RC Buildings with Smart Sensors and Wireless Network,” *Proc. of 5th World Conference on Structural Control and Monitoring*.

K.En, M.Nakamura, S.Ikegaya, T.Yanase and K.Yoneyama, 2008, “Practical Structural Health Monitoring System of Low-Cost Smart Sensors with Wireless Network,” *Proc. of 14th World Conference on Earthquake Engineering*.

T.Yanase and S.Ikegaya, 2006, “A Study on Damage Detection System Using Smart AE Sensor,” *Trans. of 2nd International Conf. on Structural Health Monitoring and Intelligent Infrastructure*, 401-406.